A Glial K/Cl Transporter Controls Neuronal Receptive-Ending Shape by Chloride Inhibition of an rGC

Aakanksha Singhvi[1], **Bingqian Liu**[2], **Christine J. Friedman**[1,3], **Jennifer Fong**[1,4], **Yun Lu**[1], **Xin-Yun Huang**[2], and **Shai Shaham**[1,*]

[1]Laboratory of Developmental Genetics, The Rockefeller University, 1230 York Avenue, New York, NY 10065 USA

[2]Department of Physiology, Cornell University Weill Medical College, 1300 York Avenue, New York, NY 10065 USA

SUMMARY

Neurons receive input from the outside world or from other neurons through neuronal receptive endings (NREs). Glia envelop NREs to create specialized microenvironments; however, glial functions at these sites are poorly understood. Here we report a molecular mechanism by which glia control NRE shape and associated animal behavior. The *C. elegans* AMsh glial cell ensheathes NREs of twelve neurons, including the thermosensory neuron AFD. KCC-3, a K/Cl transporter, localizes specifically to a glial microdomain surrounding AFD receptive-ending microvilli, where it regulates K^+ and Cl^- levels. We find that Cl^- ions function as direct inhibitors of an NRE-localized receptor-guanylyl-cyclase, GCY-8, which synthesizes cGMP. High cGMP mediates the effects of glial KCC-3 on AFD shape by antagonizing the actin-regulator WSP-1/NWASP. Components of this pathway are broadly expressed throughout the nervous system, suggesting that ionic regulation of the NRE microenvironment may be a conserved mechanism by which glia control neuron shape and function.

INTRODUCTION

Neurons receive information from the environment or other neurons through dendritic structures termed neuronal receptive-endings (NREs). In the mammalian central nervous system (CNS), postsynaptic neurons receive excitatory inputs at NREs termed spines, actin-rich receptive-endings that protrude from the dendrite shaft. Developmental and experience-dependent remodeling suggests that plasticity of spine morphology may correlate with learning and memory (Bourne and Harris, 2008). Perturbations in spine shape are associated

with disorders including epilepsy, dementia, schizophrenia, Huntington's disease, Alzheimer's disease, and Fragile X syndrome (Penzes et al., 2011). Spines are often ensheathed by astrocytic glia (Chung et al., 2015). Glial cues are implicated in spine shape control, however, mechanisms by which they regulate spine morphology *in vivo* are not well understood (Christopherson et al., 2005; Chung et al., 2015; Murai et al., 2003).

Sensory NREs are comprised of microtubule-based cilia or actin-based microvilli, and are also glia-approximated. Sensory NRE shape perturbation leads to sensory deficits and is common in patients with congenital defects such as deafness-blindness Usher's syndrome, or inherited conditions such as retinal degeneration. Genetic lesions underlying these syndromes affect sensory organ glia or associated neurons/neuron-like cells (Estrada-Cuzcano et al., 2012; Kremer et al., 2006). Glial mediators of sensory NRE shape are not known.

Glia often provide trophic support for neurons, complicating investigation of their roles in NRE shape control *in vivo*. *C. elegans* AMsh glia, which envelop neurons of the amphid sense organ, resemble mammalian glia but are dispensable for neuron survival. They are thus an excellent model to study glial control of NRE shape *in vivo* (Shaham, 2010). The AMsh glial cell ensheathes microvilli NREs of the AFD thermosensory neuron, as well as NREs of eleven other neurons, including the ciliated NRE of the AWC chemosensory neuron (Figure 1A) (Ward et al., 1975). We previously showed that ablation of AMsh glia disrupts AFD microvilli and AWC cilia NREs (Bacaj et al., 2008). Whether this reflect passive or active glial roles was unclear. Furthermore, molecules mediating glial contribution to NRE shape were unknown.

AFD NREs consist of microvilli and a single simple cilium (Figure 1A) (Doroquez et al., 2014; Perkins et al., 1986). Biogenesis of *C. elegans* cilia has been explored (Inglis et al., 2007). However, mutations in genes affecting cilium development perturb AFD-dependent thermosensation only weakly, and do not affect the length, number, or distribution of AFD microvilli (Figure S1A) (Perkins et al., 1986; Tan et al., 2007). Conversely, mutations in the gene *ttx-1* block microvilli formation and disrupt temperature sensation, but leave the AFD cilium intact (Procko et al., 2011; Satterlee et al., 2001). Thus, different molecular programs control cilium and microvilli structures, and microvilli are important for AFD-mediated thermosensation. Shape control of microvilli NREs is poorly understood in any system.

Here we report a mechanism by which a sense organ glial cell continuously regulates the shape of a microvilli-based sensory NRE, and its associated animal behavior, by regulating the NRE microenvironment. We find that an AMsh glia-expressed K/Cl co-transporter, KCC-3, regulates AFD NRE shape and *C. elegans* thermosensory behavior by controlling Cl^- levels surrounding AFD NREs. Cl^- ions directly inhibit the AFD neuron-specific receptor guanylyl cyclase (rGC) GCY-8 by binding to the conserved $S(x)_nGPxC$ motif in its extra-cellular domain. GCY-8 determines cGMP levels within AFD along with the phosphodiesterases PDE-1 and 5. High cGMP levels antagonize the actin regulator WSP-1/WASP, blocking NRE growth.

While KCC-3 affects AFD neuron shape, it is not required for AWC neuron NRE maintenance. KCC-3 localizes to a glial microdomain surrounding the AFD NRE, but not around the AWC NRE. Thus, a single glial cell discriminates between different neurons with which it associates.

Homologous and analogous components of this pathway are expressed throughout the CNS/PNS of many species. Our results suggest that ionic modulation of receptor activity at NREs may be a conserved mechanism by which glia regulate NRE shape and function.

RESULTS

Glia-secreted and/or membrane-bound factors control AFD NRE shape

To determine whether AMsh glia provide merely passive structural support, or whether active signaling promotes AFD NRE shape acquisition, we aimed to determine whether glia-secreted or membrane-bound proteins are required for AFD microvilli shape control. We generated animals containing a dominant-negative version of the ER-Golgi trafficking regulator RAB-1 (RAB-1^{S25N}) under control of the AMsh glia-specific and temperature-sensitive *ver-1* promoter. This construct is predicted to block exocytic traffic of secreted and membrane proteins at 25°C (Satoh et al., 1997). Thus, transient incubation at 25°C for 24 hours leaves glia structurally intact, but should impair signaling. Using this tool, we blocked glial secretion in young adults. A pronounced defect in AFD and AWC NRE shape was observed, mimicking the effects of glia ablations (Figure 1B, S2A). By contrast, non-transgenic animals raised at 15°C and transferred as L4 larvae to 25°C, or transgenic animals raised at 15°C (Figure 1B) have normal AFD microvilli. Thus, secreted or membrane-bound glial cues are required continuously to maintain AFD microvilli shape post-development. Glia-dependent dynamic plasticity of sensory structures had not been previously appreciated.

KCC-3 is a regulator of AFD NRE shape and function

To identify the relevant glial cues controlling AFD microvilli shape, we performed candidate mutant and RNA interference screens focused on inactivating glia-enriched genes encoding membrane or secreted proteins (Bacaj et al., 2008). We found that mutations in the *kcc-3* gene result in AFD microvilli loss (Figure 1C–F). KCC-3 encodes a predicted K/Cl co-transporter homologous to human solute carrier protein SLC12A4, a protein predicted to require RAB-1-mediated trafficking for membrane localization. A null lesion in the gene, *kcc-3*(*ok228*), results in temperature- and age- dependent loss of AFD NREs. 96-hour *kcc-3*(*ok228*) adults or *kcc-3*(*ok228*) adults grown at 15°C display more pronounced deficits than 24-hour adults or adults grown at 25°C, respectively (Figure 1F). Weaker, but similar defects accompany *kcc-3*(*tm3649*) mutants, which harbor a smaller in-frame truncation of the gene (Figure 1E,F), consistent with the severity of gene disruption.

AFD is the primary thermosensory neuron in *C. elegans*, and its NREs house proteins that mediate thermosensory transduction (Garrity et al., 2010). This transduction apparatus is also required for the ability of *C. elegans* to remember its temperature of cultivation (Mori and Ohshima, 1995). We found that *kcc-3*(*ok228*) animals exhibit deficits in thermotaxis

behavior when asked to choose their cultivation temperature on a temperature gradient. These behavior defects mirror the temperature- and age-dependence of *kcc-3*(*ok228*) AFD NRE defects (Figures 1G,H; S2B), suggesting a common underlying mechanism by which KCC-3 regulates AFD receptive-ending shape and AFD-mediated animal behavior.

The behavior and NRE shape defects we observed in *kcc-3*(*ok228*) mutants are similar to those reported for AMsh glia-ablated animals (Bacaj et al., 2008), suggesting that KCC-3 is a major mediator of the glial effect on AFD.

KCC-3 functions in AMsh glia to regulate AFD NRE shape

To confirm that KCC-3 is expressed in AMsh glia, we examined animals carrying a *kcc-3* [5'UTR::gfp::3'UTR] transgene (Tanis et al., 2009). *kcc-3* expression is detected exclusively in glia, including AMsh glia, but not in AFD (Figure 2A,B). Expression of *kcc-3* coding sequences under the same 5' UTR, or expression of a *kcc-3* cDNA under control of a heterologous AMsh glia-specific promoter rescued *kcc-3*(*ok228*) AFD neuron shape defects (Figure 2C). Thus, KCC-3 functions specifically in AMsh glia to control AFD NRE shape.

KCC-3 localization is restricted to a glial micro-domain surrounding AFD NREs

AMsh glia ensheath sensory NREs of other neurons, such as AWC, in addition to those of AFD. Furthermore, AMsh glia ablation or exocytosis block with RAB-1^{S25N} disrupts NRE structure of these neurons (Figure S2A) (Bacaj et al., 2008). Thus, a general mechanism may underlie NRE shape control by glia. Surprisingly, however, we found that *kcc-3* mutations do not affect AWC NREs (Figure S2A,C,D). To investigate the origin of this specificity, we examined KCC-3 subcellular localization using a genomic fosmid clone containing the *kcc-3* locus recombineered with GFP immediately upstream of the *kcc-3* stop codon, or a clone in which a *kcc-3* cDNA is tagged with mCherry and expressed under an AMsh glia-specific promoter. We found that KCC-3 localizes to the portion of the AMsh glia apical domain in which AFD microvilli are embedded, and is conspicuously absent from the region surrounding AWC or any other amphid neuron (asterisk, Figure 2D,E). Restricted localization, therefore, likely explains the specific effects of KCC-3 on AFD receptive-endings.

Thus, contrary to our initial assumption, the AMsh glial cell employs different molecular mechanisms to control AFD and AWC receptive-ending shape. While single glial cells in other systems also contact multiple neurons, whether they discriminate between these neurons has been a major outstanding question. Our results provide definitive *in vivo* evidence that they can do so.

Glial KCC-3 regulates AFD NRE shape by regulating K$^+$ and Cl$^-$ levels

KCC channels transport K$^+$ and Cl$^-$ ions across membranes (Russell, 2000). We wondered, therefore, whether ionic imbalance may underlie AFD defects in *kcc-3*(*ok228*) mutant animals. To test this, we compared AFD receptive-ending defects in *kcc-3*(*ok228*) mutants cultivated on standard *C. elegans* growth medium, and those raised on plates supplemented with 150 mM KCl. Remarkably, AFD microvilli morphology in *kcc-3*(*ok228*) mutants raised on high KCl was largely normal (Figure 2F). Rescue of the *kcc-3* mutant defects

could also be achieved acutely, as 72-hour animals transferred to KCl-supplemented plates showed significant rescue within 24 hours (Figure 2F, "KCl-acute").

To determine whether both K^+ and Cl^- were required for rescue, we raised *kcc-3(ok228)* mutants on plates supplemented with 150 mM Na^+Cl^- or $K^+Acetate^-$. While modest rescue was seen in younger animals in both cases, this was not sustained in older ones (Figure 2F).

Thus, K^+ and Cl^-, regulated by KCC-3, are acutely required to control AFD microvilli shape. Furthermore, the specific localization of KCC-3 to glial membranes around AFD strongly suggests that these ions function in the vicinity of the AFD NRE.

KCC-3 regulates AFD NRE shape through the AFD-specific rGC, GCY-8

AFD neuronal activity requires a cyclic nucleotide gated channel (CNG) composed of the TAX-2 β subunit and the TAX-4 or CNG-3 α subunits (Cho et al., 2004; Coburn and Bargmann, 1996; Komatsu et al., 1996). CNG channels allow cations (Na^+, K^+, and Ca^+) to flow across membranes down their electrochemical gradients. Our finding that medium supplementation with K-acetate fails to rescue *kcc-3(ok228)* mutants suggested that impaired K^+ conductance through these cation channels is unlikely to fully explain the AFD NRE defects of these mutants. To test this directly, we examined *tax-4* and *cng-3* single mutants, or *tax-4; cng-3* double mutants. We found that these animals have only minor defects in AFD microvilli length, with some exhibiting elongated and disorganized microvilli (Figure 2G; hatched bars). Furthermore, mutations in genes functioning in downstream interneurons (*ttx-3*), or in adaptation of other neurons (*egl-4*) also have no effect on AFD shape (Figure S1B). Thus, the effects of KCC-3 on AFD shape cannot be entirely explained by reduced CNG channel conduction, and appear independent of downstream circuit dynamics.

We considered the possibility that glial KCC-3 defects could lead to increased K^+ and Cl^- accumulation in the extracellular space surrounding AFD microvilli, leading to hyperactive signaling through CNG channels. If this were the case, CNG channel mutations should mitigate the AFD shape defects of *kcc-3(ok228)* mutants. However, we found that *tax-4* mutations did not suppress *kcc-3(ok228)* defects at all (Figure 2G). Our data, therefore, suggest that neuronal activity is not the primary effector of KCC-3 for AFD microvilli shape control. We therefore sought another neuronal effector.

CNG channels are activated by cGMP, synthesized by receptor guanylyl cyclases (rGCs). rGCs are Type I transmembrane proteins with extracellular (ECD), transmembrane (TM), kinase-homology (KHD), hinge (H), and guanylyl cyclase catalytic (CAT) domains (Figure 3A). The AFD neuron expresses the rGCs GCY-8, -18, and -23, which function redundantly to regulate thermotaxis behavior (Inada et al., 2006; Yu et al., 1997). We examined *gcy-8(tm949)*, *gcy-18(nj38)*, and *gcy-23(ok797)* single loss-of-function mutants and found no defects in AFD receptive-ending shape. Remarkably, however, the *gcy-8(tm949)* lesion, predicted to eliminate GCY-8 cyclase activity, strongly mitigates the AFD microvilli defects of *kcc-3(ok228)* mutants (Figures 3B, S3). This effect is largely specific to *gcy-8*, as the *gcy-23(ok797)* loss-of function allele only weakly rescues the AFD NRE defects of *kcc-3(ok228)* mutants (Figure 3B). Intriguingly, a genomic fosmid, in which GFP sequences

are fused just upstream of the *gcy-8* stop codon, is expressed specifically in AFD, and GFP fluorescence is localized to AFD microvilli (Figure S4A), consistent with previous studies.

Together, our studies suggest that GCY-8 is a key effector of KCC-3, and that loss of KCC-3 results in an increase in GCY-8 activity.

Increased GCY-8 activity, through KHD inactivation, blocks AFD NRE extension

The hypothesis that increased GCY-8 activity mediates the effects of glial *kcc-3* lesions was serendipitously corroborated by results of a genetic screen we conducted seeking mutants with defective AFD microvilli. From 10,800 F2 progeny examined (3.5 genomes), we recovered six relevant mutants. Genetic mapping, whole-genome sequencing, and transformation rescue studies revealed that one of these, *ns335*, has a causal lesion in *gcy-8*. The *gcy-8(ns335)* mutation is predicted to cause a G707E change in a highly conserved D(F/H/Y)G motif within the kinase homology domain (Figures 3A,C; S3A). This lesion has not been previously described in other rGCs.

Fluorescence microscopy revealed that *gcy-8(ns335)* mutants have fewer and shorter AFD microvilli (Figure 3D), and we confirmed this using serial-section transmission electron microscopy (TEM) (Figure 3E,F) and focused ion beam scanning EM (FIB-SEM)(Figure 3G,H; Movies S1–S4). Using TEM, we found that while wild-type AFD neurons have 43 ± 2 microvilli (n=6), *gcy-8(ns335)* mutants have 12 ± 1 (n=4) microvilli. SEM image analysis showed maximal microvilli length of 2.5 μm for wild-type animals, but only 1.5 μm for *gcy-8(ns335)*.

gcy-8(ns335)/+ heterozygotes do not show AFD NRE abnormalities, and the defects of *gcy-8(ns335)* homozygotes are rescued by expression of wild-type genomic sequences (Figure 3I), demonstrating that *ns335* is a recessive allele. However, *gcy-8(tm949)* mutants, lacking the GCY-8 cyclase domain, have no effect on AFD microvilli shape, and suppress *kcc-3(ok228)* mutant defects (Figure 3B). Thus, *gcy-8(ns335)* is unlikely to be a loss-of-function allele.

Supporting this idea, while *gcy-8(tm949)* mutants have near normal thermotaxis behavior on a linear thermal gradient (Wasserman et al., 2011), *gcy-8(ns335)* mutants accumulate at low temperatures (15°C) regardless of their cultivation temperature (Figure 3J,K). Furthermore, unlike *gcy-8(tm949)*, the *gcy-8(ns335)* allele does not suppress the AFD NRE shape defects of *kcc-3(ok228)* (Figure S4B). Thus, *gcy-8(ns335)* appears to be a gain of GCY-8 function. The recessive nature of *gcy-8(ns335)* could be explained by the observation that rGC dimerization is essential for function (Potter, 2011). Formation of heterodimeric mutant/wild-type GCY-8 complexes in *gcy-8(ns335)*/+ heterozygotes would be predicted to reduce cyclase activity. Indeed, expression of a cyclase-dead GCY-8^{D976A} protein in AFD can rescue *gcy-8(ns335)* microvilli defects (Figure 4A), presumably by promoting non-productive dimer formation as is the case for equivalent mutations in other rGCs (Thompson and Garbers, 1995).

The *gcy-8(ns335)* mutation results in a G707E substitution in a conserved D(F/H/Y)G motif in the kinase-homology domain (KHD) of GCY-8 (Figures 3A,C; S3A). Deletion of the

KHD of the human rGC NPR1 enhances cyclase activity in cell-culture experiments (Koller and Goeddel, 1992). Thus, the *gcy-8(ns335)* mutation may block the inhibitory effect of the KHD domain on cyclase activity. To understand the role of the KHD, we first developed an *in vivo* assay for GCY-8 function. Specifically, we found that overexpression of a GCY-8 cDNA in AFD neurons of otherwise wild-type animals using an AFD promoter::*gcy-8* cDNA plasmid injected at high copy promotes microvilli loss (Figure 4A). Thus, increased GCY-8 activity leads to AFD NRE loss. Furthermore, expression of full-length GCY-8 containing an E1057A mutation, whose equivalent hyper-activates other rGCs (Wedel et al., 1997), weakly but significantly exaggerated the effects of wild-type GCY-8 overexpression (Figure 4A). We also generated wild-type animals expressing the cyclase-dead GCY-8[D976A] protein. This single amino-acid substitution curtailed the ability of GCY-8 overexpression to block microvilli growth (Figure 4A).

To test the effect of the KHD domain on cyclase activity, we first showed that overexpressing a fragment of GCY-8 consisting only of the HCAT domain was sufficient to elicit AFD microvilli defects (Figure 4A). Similar constructs for other rGCs have constitutive cyclase activity in cell culture studies (Thompson and Garbers, 1995). As expected if *gcy-8(ns335)* is a gain-of-function allele, expression of the hyper-activated GCY-8 HCAT fragment fails to rescue *gcy-8(ns335)* defects (Figure 4A). However, AFD microvilli NRE loss was abrogated if the HCAT domain was fused to the KHD domain, with or without the transmembrane domain (KHD-HCAT or TM-KHD-HCAT) (Figure 4B). Of note, while the TM-KHD-HCAT protein rescues *gcy-8(ns335)*, the KHD-HCAT protein fragment does so significantly less efficiently (Figure 4B), suggesting that membrane localization of GCY-8 is important for its dimerization and cyclase activity regulation. Our results suggest that elevated cyclase activity, effected by inhibition of the KHD domain, blocks AFD NRE extension.

Our findings also suggest that the conserved DFG motif, mutated in *gcy-8(ns335)* animals, and present in the KHD of all rGCs is likely the relevant element mediating cyclase inhibition by the KHD domain *in vivo.*

GCY-8 functions downstream of KCl

As is the case for *kcc-3* mutants, the effect of *gcy-8(ns335)* on AFD microvilli structure is largely independent of AFD neuron function, as *tax-4* mutations fail to suppress *gcy-8(ns335)* AFD microvilli defects (Figure 3L). Importantly, dietary supplementation with KCl does not rescue *gcy-8(ns335)* NRE shape defects (Figure S4B).

Thus, rescue of *kcc-3(ok228)* NRE shape defects by exogenous KCl is not due to non-specific effects on neuron morphology. Furthermore, GCY-8 functions downstream of KCC-3 and KCl, as would be predicted for a KCC-3 effector.

GCY-8 has a ligand-independent basal cyclase activity inhibited by the DFG motif

Our finding that glial *kcc-3* mutant defects can be overcome by inactivating GCY-8 in AFD neurons suggests that GCY-8 may have constitutive cyclase activity that is inhibited by KCC-3. Consistent with this idea, we found that overexpression of either GCY-8 or the orphan human retinal rGC GUCY2D, previously shown to have basal activity (Duda et al.,

1996; Shyjan et al., 1992), promotes AFD microvilli loss in wild-type animals (Figure 4C). However, expression of the human rGC NPR-1, which requires ANP peptide for activity, or the rGC scavenger receptor, NPR-3, lacking a cyclase domain, had negligible effects on AFD shape (Figure 4C).

To directly test whether GCY-8 has basal activity, we generated stably-integrated HEK293T cell lines expressing wild-type or mutant versions of hNPR-1 or GCY-8 proteins, and assayed these for steady-state cGMP levels (Figure 5A,B). We draw three important conclusions from these studies. First, while hNPR1 has essentially no basal activity, as previously reported, GCY-8-expressing cells show significant activity, as predicted by our genetic data. Second, consistent with our *in vivo* studies, GCY-8^{G707E}, which affects the conserved DFG motif in the KHD domain, enhances this basal cyclase activity, similar to or greater than an activating lesion previously described in other rGCs (GCY-8^{E1057A}). Third, the GCY-8^{G707E}-analogous mutation in hNPR1 (hNPR1^{G680E}) also shows increased cyclase activity. Thus, GCY-8 has basal cyclase activity and the glycine residue of the DFG motif is important for cyclase inhibition across rGCs.

Cl⁻ ions inhibit GCY-8

Our data raise the possibility that KCC-3 may inhibit GCY-8 through the action of K^+ or Cl^-. To test whether this effect is direct and which ion can inhibit GCY-8 activity, we performed reconstituted membrane fraction assays using the stably integrated HEK293T cell lines described above. As with the whole cell assays, we found a 2.7-fold increase in cGMP production in GCY-8 containing fractions (Figure 5C). Strikingly, we found that Cl^- ions, but not K^+ or other anions, are potent inhibitors of GCY-8 cyclase activity and cGMP production (Figures 5D, S5A), with an IC_{50} of ~60mM. This IC_{50} is within the physiological range for extracellular Cl^- concentrations in many settings (Tora et al., 2015), suggesting that changes in extracellular Cl^-, as would be predicted to occur in *kcc-3* mutants, should indeed affect GCY-8 activity. Consistent with these *in vitro* results, we found that exogenous supplementation with Cl^- mitigates the over-expression defects of GCY-8 *in vivo* (Figure 5E). Also, previous studies suggest that cGMP levels may be reduced at lower temperatures to allow CNG channels in AFD to close as part of the thermosensory response (Garrity et al., 2010). Thus, defects in inhibition of cGMP production by GCY-8 should be more pronounced at 15°C, which is exactly what we see in null *kcc-3* mutants (Figure 1F). Taken together, our results support a model in which KCC-3 regulates extracellular Cl^- levels, which, in turn, directly influence GCY-8 guanylyl cyclase activity.

Cl⁻ inhibits GCY-8 by binding to a functionally conserved Cl– binding motif in its ECD

Crystal structures of the rat rGC NPR1 reveal a Cl^- in the ECD domain within a pocket defined by the motif $S(x)_nGPxC$ (van den Akker et al., 2000; Ogawa et al., 2010). A conserved $S(x)_nGPxC$ motif is present in the ECD of GCY-8 (Figure S5B,C), but not in GCY-23, mutations in which suppress *kcc-3* lesions only modestly (Figures 3B, S5C). The $S(x)_nGPxC$ motif is structurally conserved in the ECD of metabotropic glutamate receptors (mGluRs), and Cl^- is an orthosteric ligand for mGluRs (DiRaddo et al., 2015; Tora et al., 2015). Of note, the IC_{50} for Cl^- inhibition of GCY-8 is identical to the Cl^- EC_{50} measured

for mGluR2 activity, consistent with a possible role for the GCY-8 $S(x)_nGPxC$ ECD motif in mediating the effects of Cl^-.

Supporting this idea, exogenous *in vivo* supplementation with Cl^- salts does not suppress the over-expression defects of the HCAT fragment lacking the ECD, but suppresses defect of full-length GCY-8 overexpression (Figure 5E). Furthermore, mutating the conserved Cl^- binding domain serine of mGluRs to glutamate mimics the effects of Cl^- (Dutzler, 2003; Tora et al., 2015). We found that a similar mutation in GCY-8 (GCY-8^{S110E}) inhibits the ability of GCY-8 to promote NRE involution *in vivo* (Figure 5F), suggesting that this motif may indeed be functionally conserved. To confirm this, we expressed GCY-8^{S110E} in HEK293T cells and measured basal guanylyl cyclase activity in reconstituted membrane fractions. GCY-8^{S110E} had reduced basal activity compared to GCY-8, as expected of a mutation that mimics binding of an inhibitory Cl^- ligand (Figure 5G). Furthermore, GCY-8^{S110E} was insensitive to increasing levels of Cl^-, unlike full length GCY-8 (Figure 5H). By contrast, the GCY-8^{G707E} and GCY-8^{E1057A} activated proteins that possess intact ECDs retain Cl^- inhibition, but with dampened efficacy compared to full-length GCY-8 (Figure 5H).

Changing the conserved cysteine of the $S(x)_nGPxC$ motif to serine enhances Cl^- coordination in mGluRs by introducing a second hydroxyl moiety into the Cl^- binding pocket (Figure S5B, C) (Tora et al., 2015). We found that the same may be true for the $S(x)_nGPxC$ motif of GCY-8. GCY-8^{C141S} slightly reduces the ability of GCY-8 to prevent NRE extension *in vivo* (Figure 5F), and shows reduced basal activity compared to GCY-8 (Figure 5G) and reduced Clsensitivity *in vitro* (Figure 5H).

Taken together, these results suggest that Cl^- ions directly inhibit GCY-8 activity by binding to the conserved $S(x)_nGPxC$ motif in the extra-cellular domain of GCY-8.

Excess cGMP blocks AFD NRE growth

Our studies suggest the hypothesis that increased cGMP production by GCY-8 promotes AFD NRE disappearance. To examine the involvement of cGMP in AFD NRE shape control, we reasoned that GCY-8-independent manipulations that alter cGMP levels within AFD should also alter microvilli morphology. Therefore, we expressed cyclase-activated forms of human NPR-1 (hNPR-1^{E1006A}) and human GUCY2D (hGUCY2D^{E1010A}, a retinal rGC) in the AFD neuron (Wedel et al., 1997). As shown in Figure 4C, transgenic animals display defects in microvilli extension, suggesting that excess cGMP produced by these heterologous guanylyl cyclases indeed blocks AFD NRE growth. Similarly, hGUCY2D protein containing a lesion homologous to the GCY-8^{G707E} lesion (hGUCY2D^{G686E}), also significantly shortens AFD receptive-ending microvilli (Figure 4C).

As an alternate means of modulating cGMP levels, we examined the consequences of changing the activities of phosphodiesterase (PDE) genes, encoding proteins that degrade cGMP, on AFD receptive-ending morphology. *C. elegans* has four such genes (*pde-1, -2, -3, -5*) (Liu et al., 2010), two of which (*pde-2*, and *-5*) are known to be expressed in AFD (Wang et al., 2013). While a *pde-1* gene reporter containing limited 5' regulatory sequences fused to GFP was not previously detected in AFD (Wang et al., 2013), we found that a fosmid

derived from genomic DNA surrounding the locus, and recombineered to introduce GFP coding sequences just upstream of the *pde-1* stop codon, is expressed in the cell (Figure S6C). Thus, at least 3 PDEs are expressed in AFD.

A quadruple mutant inactivating all cGMP PDE genes showed complete loss of AFD microvilli (Figure 6A). A *pde-5 pde-1* double mutant also displayed a fully penetrant loss of AFD receptive-endings (Figure 6A). Single, double, or triple combinations of mutations in the other cGMP PDE genes or in the cAMP-specific PDE gene, *pde-4*, had no effect on AFD receptive-ending shape (Figure S6A). Thus, PDE-1 and PDE-5 are the only PDEs required for AFD microvilli extension, and appear to function redundantly. We conclude that PDE-1 and PDE-5 likely act cell autonomously in the AFD neuron to regulate receptive-ending shape, and that excess cGMP blocks microvilli extension.

To test whether increasing PDE activity reciprocally promotes AFD microvilli elongation, we examined *pde-5 pde-1* double mutants expressing a cDNA derived from the *pde-1*B mRNA isoform, in AFD (Figure S6B). This transgene strongly rescues the AFD defects of the double mutant (Figure 6A), supporting the idea that PDE-1 and PDE-5 exercise interchangeable cell-autonomous activities required for AFD morphogenesis. Furthermore, PDE-1B overexpression restores AFD NRE microvilli to *kcc-3*(*ok228*) and *gcy-8*(*ns335*) mutants, consistent with the idea that high cGMP levels block microvilli elongation in these mutants (Figure 6A). Importantly, we noticed that in some animals overexpressing PDE-1B, microvilli are longer than in the wild type, and are sometimes misshapen (Figures 6A, gray bars; S6D,E). Our results suggest, therefore, that cGMP levels are sufficient to dictate the extent of microvilli elongation.

cGMP antagonizes the actin regulator WSP-1 to control AFD receptive-ending shape

Since the effects of cGMP on AFD NRE shape are largely independent of CNG channels, we sought to identify a relevant mediator for shape determination. From a screen of candidate effectors, we found that overexpression in otherwise wild-type AFD neurons of a cDNA corresponding to the gene *wsp-1*, encoding the well-studied actin regulator NWASP, results in elongated AFD microvilli (Figures 6B, S7A,B), suggesting that WSP-1 promotes microvilli formation. Strikingly, WSP-1 overexpression restores microvilli to *gcy-8*(*ns335*) mutants (Figure 6B). A similar result is obtained using a genomic clone carrying the *wsp-1* gene (Figure 6B). These observations suggest that high cGMP inhibits microvilli growth by antagonizing WSP-1. Supporting the idea that WSP-1 is normally required for AFD NRE growth, *wsp-1*(*gm324*) mutants homozygous for a loss-of-function mutation perturbing the *wsp-1*A mRNA isoform are defective in AFD microvilli elongation. Moreover, *wsp-1(gm324)* animals also show defects in thermotaxis behavior at all temperatures and ages tested (Figure 6D–F). Another allele, *wsp-1(gk208630)*, which only affects the *wsp-1*B isoform, does not affect AFD NREs (Figure S7C,D).

We note that wild-type animals over-expressing WSP-1A occasionally display shorter microvilli (Figure 6B). One explanation for this may be that high levels of WSP-1 target free actin to new filament ends, preventing elongation of existing filaments (Smith et al., 2013a). Consistent with this hypothesis, double mutants between *gcy-8*(*tm949*) and *gcy-23*(*ok797*)

null alleles show a modest reduction in microvilli length, as do some animals overexpressing PDE-1B (Figure 6A,C).

The finding that *wsp-1*(*gm324*) animals exhibit a weaker NRE defect than *gcy-8*(*ns335*) mutants suggests that a second actin polymerizing factor also functions downstream of cGMP. Importantly, however, the ability of WSP-1 overexpression alone to promote AFD microvilli elongation in wild type animals, and rescue the defects of *gcy-8(ns335)*, demonstrates that actin nucleation in AFD actin-rich microvilli is likely the key step that is being regulated by the glia-neuron interactions we uncovered. We therefore conclude that cGMP antagonizes WSP-1 activity, which likely regulates nucleation of actin filaments in AFD NREs. These results also imply that unexpectedly, we have found that cGMP regulates at least two independent effectors – CNG channels and WSP-1, with different functions in the AFD neuron, and WSP-1 is the key downstream effector for regulation of AFD NRE shape.

DISCUSSION

Our studies identify a glial regulator of sensory NRE shape, and reveal that glia can dictate NRE shape by controlling the NRE microenvironment. Our findings support a model (Figure 7) in which the glial K/Cl transporter KCC-3 localizes around and controls Cl⁻ levels surrounding AFD microvilli. Cl⁻ inhibits the AFD-specific rGC GCY-8, which has a conserved Cl⁻ binding structural motif. GCY-8, along with PDE-1 and PDE-5, modulate neuron cGMP levels, and cGMP antagonizes WSP-1, which promotes NRE elongation, presumably through actin nucleation. Importantly, our studies reveal that glia continuously maintain AFD NRE shape, presumably by regulation of the microenvironment.

Glia discriminate among NREs

Our findings that KCC-3 localizes around AFD NREs and is selectively required for their function, demonstrate that a single glial cell discriminates between neurons with which it associates by targeting regulators to specific neuron-contact sites. Mammalian astrocytes can associate with 100,000 NREs (Chung et al., 2015), and Ca²⁺ fluxes in astrocytes have localized features (Khakh and Sofroniew, 2015). We suggest that the ability to discriminate between associated neurons may be a universal property of glia. Understanding how KCC-3 localization is achieved may provide a molecular handle on targeted control of neurons by glia.

Glia control sensory and synaptic NRE shape and function

How actin-based microvilli NREs are formed and maintained has not been explored. Our results will likely apply to many such sensory structures. Indeed, glia/glia-like cells regulate the ionic milieu of diverse actin-based sensory NREs, and human disease mutations affect these cells (Estrada-Cuzcano et al., 2012; Hamel, 2007). KCC and NKCC co-transporters are expressed in glia of the ear, retina, and in Schwann cells (Boettger et al., 2002; Kettenmann and Verkhratsky, 2008), and their disruption can lead to NRE degeneration (Gallemore et al., 1997; Strauss, 2005). KCC3 loss in humans leads to sensory neuropathy (Kahle et al., 2015).

rGCs are also widely expressed in sensory and other neuron types, and retinal GUCY2D and Grueneberg ganglion GC-G have basal guanylyl cyclase activities similar to GCY-8 (Chao et al., 2015; Shyjan et al., 1992). Increased GUCY2D activity leads to defects in photoreceptor outer segment shape in Leber's Congenital Amaurosis with some patient mutations mapping to the ECD (Perrault et al., 2000). These effects are reminiscent of the effects of GCY-8^{G707E} on AFD NREs.

Our work may also present a paradigm for understanding glial effects on spine morphology in the CNS. Astrocytic KCC channels regulate K/Cl levels in the CNS (Kettenmann and Verkhratsky, 2008). Disruption of K/Cl levels contributes to neuronal dysfunction in Huntington's disease and epilepsy models (Kahle et al., 2015; Tong et al., 2014), and to defects in spine shape (Murmu et al., 2015).

AMsh glia form a bounded compartment around AFD NREs, which, as in synapses, allows tight control of the NRE milieu. A role for extracellular Cl$^-$ in modulating spine-localized metabotropic glutamate receptors has been explored (Tora et al., 2015). Our studies suggest that in addition to providing a diffusion barrier, glia may actively control synaptic Cl$^-$ levels to modulate spine activity and shape. Supporting this proposition, mGluRs (Class III GPCRs) and rGCs adopt a LIVBP (Leu/IsoLeu/Val binding periplasmic protein-like) fold in the extracellular domain (Acher et al., 2011). The $S(x)_n GPxC$ Cl$^-$ binding motif is conserved across nervous system LIVBP fold receptors (Acher et al., 2011).

Glial control of thermosensation

Electrophysiological studies of AFD neurons suggest that high/low cGMP opens/closes CNG channels upon warming/cooling (Garrity et al., 2010; Ramot et al., 2008) relative to the cultivation temperature. Thus, within the operating range of the thermosensory apparatus, a basal level of cGMP must exist that can be modulated up or down. That GCY-8 has basal activity supports this idea, as does our observation that *kcc-3* mutants exhibit more pronounced thermosensory deficits at low temperature, where higher GCY-8 inhibition may be required.

We previously showed that expression of the VER-1 receptor tyrosine kinase in AMsh glia is temperature dependent and independent of the AFD neuron (Procko et al., 2011). It is possible that modulation of AMsh glia-dependent properties, such as KCC-3 activity, by temperature may also form part of the thermosensory apparatus.

Control of rGC activity

rGCs are prevalent receptors and are important therapeutic targets (Potter, 2011). Our data highlight unexpected aspects of rGC structure and function. That neuronal rGCs (e.g. GCY-8, GUCY2D) have basal activities but non-neuronal rGCs (e.g. NPR-1 and NPR-2) do not, suggests the possibility of a fundamental dichotomy. The identification of Cl$^-$ as a GCY-8 inhibitor raises the possibility that rGCs with basal activity, for which activating ligands have not been identified, may instead be regulated by inhibitory extracellular cues. Our results suggest that the relationship between the ECD and KHD may be inverted in rGCs with basal activity vs. ligand-activated non-neuronal rGCs.

That Cl^- ions influence GCY-8 activity also suggests that other ion may control rGCs. A recent study exploring rGCs in K^+ and I^- sensation in *C. elegans* revealed that stimulus specificity tracks with receptors ECDs (Smith et al., 2013b). Thus, rGCs may sense different ions through their ECD.

Finally, we show that a conserved glycine residue in the KHD has inhibitory roles in GCY-8 and also in human NPR1. The D(F/H/Y)G motif containing this amino acid is conserved in all kinases and pseudo-kinases and forms part of the activation loop. Thus, this domain may facilitate ATP binding, previously suggested to affect rGC activity (Goraczniak et al., 1992).

EXPERIMENTAL PROCEDURES

C. elegans methods

Standard culturing and germ-line transformation methods were used (Brenner, 1974; Mello and Fire, 1995). Mutants, transgenes, genetic methods, RNAi methods and thermotaxis assays are described in Supplemental Methods.

Plasmids

Plasmid construction details are provided in Supplemental Methods.

Microscopy and Image Processing

Images were collected on an Axioplan 2 microscope (Zeiss) with 63x/1.4 NA objective (Zeiss) and dual-band filter set (Chroma, Set 51019). Some images were collected on a DeltaVision Core imaging system (Applied Precision) with a PlanApo 603/1.42 NA or UPLSApo 1003/1.40 NA oil-immersion objective and a Photometrics CoolSnap HQ camera (Roper Scientific). Images were de-convolved using ImageJ. Electron microscopy methods are described in Supplemental Methods.

cGMP ELISAs

ELISAs were performed using the Direct cGMP kit (Enzo Life Sciences, ADI-900-014). 5×10^5 cells were grown on poly-D-Lysine coated plates (Corning BioCoat, 354414) for 12 hours, rinsed in D-PBS and incubated in serum free medium supplemented with 0.5 mM IBMX at 23°C or 37°C with 5% CO_2 for one hour. Cells were lysed in 0.1 M HCl + 0.1% Triton X-100 and assayed for cGMP concentration as per manufacturer's protocol (Enzo Life Sciences) (Guo et al., 2007, 2009). Optical density measurements were performed on a BioTek Synergy NEO using the Gen5 Data Analysis software. All GCY-8 experiments were performed in biological quadruplicate and NPR-1 experiments in biological triplicate. Importantly, the assay measures steady-state accumulation of cGMP (production minus degradation), and is always an underestimate of cGMP production. Membrane assays were carried out as follows: Cells were cultured in growth medium to ~95% confluency and washed in 50 mM NH_4Ac and 200 mM sucrose pH 7 (plus 1 mM IBMX and protease inhibitors). Cells were passed through a 26 gauge needle several times and sonicated for 10 seconds. After centrifugation at 2000 rpm for 5 min, membrane fraction was prepared by centrifugation at 100,000 g for 1.5 h at 4°C. The membrane pellet was resuspended in 50 mM NH_4Ac, 200 mM Sucrose pH 7, 1 mM DTT, 10 mM $MgAc_2$ and 1 mM $MnSO_4$.

Membrane preparations were treated with KCl, KAc, or NH_4Cl. 5 mM GTP was added to start the cyclase reaction. After 30 min at 30°C, membrane preparations were lysed in 0.2 M HCl and assayed for cGMP.

Supplementary Material

Refer to Web version on PubMed Central for supplementary material.

Acknowledgments

REFERENCES

Acher FC, Selvam C, Pin J-P, Goudet C, Bertrand H-O. A Critical Pocket Close to the Glutamate Binding Site of mGlu Receptors Opens New Possibilities for Agonist Design. Neuropharmacology. 2011; 60:102–107. [PubMed: 20621106]

Bacaj T, Tevlin M, Lu Y, Shaham S. Glia are essential for sensory organ function in C. elegans. Science. 2008; 322:744–747. [PubMed: 18974354]

Boettger T, Hübner Ca, Maier H, Rust MB, Beck FX, Jentsch TJ. Deafness and renal tubular acidosis in mice lacking the K-Cl co-transporter Kcc4. Nature. 2002; 416:874–878. [PubMed: 11976689]

Bourne JN, Harris KM. Balancing structure and function at hippocampal dendritic spines. Annu. Rev. Neurosci. 2008; 31:47–67. [PubMed: 18284372]

Brenner S. The genetics of Caenorhabditis elegans. Genetics. 1974; 77:71–94. [PubMed: 4366476]

Chao Y, Chen C, Lin Y, Breer H, Fleischer J. Receptor guanylyl cyclase-G is a novel thermosensory protein activated by cool temperatures. 2015; 34:294–307.

Cho SW, Choi KY, Park CS. A new putative cyclic nucleotide-gated channel gene, cng-3, is critical for thermotolerance in Caenorhabditis elegans. Biochem. Biophys. Res. Commun. 2004; 325:525–531. [PubMed: 15530424]

Christopherson KS, Ullian EM, Stokes CCa, Mullowney CE, Hell JW, Agah A, Lawler J, Mosher DF, Bornstein P, Barres Ba. Thrombospondins are astrocyte-secreted proteins that promote CNS synaptogenesis. Cell. 2005; 120:421–433. [PubMed: 15707899]

Chung W-S, Welsh CA, Barres BA, Stevens B. Do glia drive synaptic and cognitive impairment in disease? Nat. Neurosci. 2015; 18:1539–1545. [PubMed: 26505565]

Coburn CM, Bargmann CI. A putative cyclic nucleotide-gated channel is required for sensory development and function in C. elegans. Neuron. 1996; 17:695–706. [PubMed: 8893026]

Doroquez DB, Berciu C, Anderson JR, Sengupta P, Nicastro D. A high-resolution morphological and ultrastructural map of anterior sensory cilia and glia in Caenorhabditis elegans. Elife. 2014; 3:e01948. [PubMed: 24668170]

Duda T, Goraczniak R, Surgucheva I, Rudnicka-Nawrot M, Gorczyca Wa, Palczewski K, Sitaramayya A, Baehr W, Sharma RK. Calcium modulation of bovine photoreceptor guanylate cyclase. Biochemistry. 1996; 35:8478–8482. [PubMed: 8679607]

Dutzler R. Gating the Selectivity Filter in ClC Chloride Channels. Science (80-.). 2003; 300:108–112.

Estrada-Cuzcano A, Roepman R, Cremers FPM, Hollander AIDen, Mans Da. Non-syndromic retinal ciliopathies: Translating gene discovery into therapy. Hum. Mol. Genet. 2012; 21

Gallemore RP, Hughes Ba, Miller SS. Retinal pigment epithelial transport mechanisms and their contributions to the electroretinogram. Prog. Retin. Eye Res. 1997; 16:509–566.

Garrity, Pa; Goodman, MB.; Samuel, AD.; Sengupta, P. Running hot and cold: behavioral strategies, neural circuits, and the molecular machinery for thermotaxis in C. elegans and Drosophila. Genes Dev. 2010; 24:2365–2382. [PubMed: 21041406]

Goraczniak RM, Duda T, Sharma RK. A structural motif that defines the ATP-regulatory module of guanylate cyclase in atrial natriuretic factor signalling. Biochem. J. 1992; 282(Pt 2):533–537. [PubMed: 1347681]

Guo D, Tan YC, Wang D, Madhusoodanan KS, Zheng Y, Maack T, Zhang JJ, Huang XY. A Rac-cGMP Signaling Pathway. Cell. 2007; 128:341–355. [PubMed: 17254971]

Guo D, Zhang JJ, Huang XY. Stimulation of guanylyl cyclase-D by bicarbonate. Biochemistry. 2009; 48:4417–4422. [PubMed: 19331426]

Hamel CP. Cone rod dystrophies. Orphanet J. Rare Dis. 2007; 2:7. [PubMed: 17270046]

Inada H, Ito H, Satterlee J, Sengupta P, Matsumoto K, Mori I. Identification of guanylyl cyclases that function in thermosensory neurons of Caenorhabditis elegans. Genetics. 2006; 172:2239–2252. [PubMed: 16415369]

Inglis PN, Ou G, Leroux MR, Scholey JM. The sensory cilia of Caenorhabditis elegans. WormBook. 2007:1–22. [PubMed: 18050505]

Kahle KT, Khanna AR, Alper SL, Adragna NC, Lauf PK, Sun D, Delpire E. K-Cl cotransporters, cell volume homeostasis, and neurological disease. Trends Mol. Med. 2015; 21:513–523. [PubMed: 26142773]

Kettenmann H, Verkhratsky A. Neuroglia: the 150 years after. Trends Neurosci. 2008; 31:653–659. [PubMed: 18945498]

Khakh BS, Sofroniew MV. Diversity of astrocyte functions and phenotypes in neural circuits. Nat. Neurosci. 2015; 18:942–952. [PubMed: 26108722]

Koller KJ, Goeddel DV. Molecular biology of the natriuretic peptides and their receptors. Circulation. 1992; 86:1081–1088. [PubMed: 1327579]

Komatsu H, Mori I, Rhee JS, Akaike N, Ohshima Y. Mutations in a cyclic nucleotide-gated channel lead to abnormal thermosensation and chemosensation in C. elegans. Neuron. 1996; 17:707–718. [PubMed: 8893027]

Kremer H, van Wijk E, Märker T, Wolfrum U, Roepman R. Usher syndrome: Molecular links of pathogenesis, proteins and pathways. Hum. Mol. Genet. 2006; 15:262–270.

Liu J, Ward A, Gao J, Dong Y, Nishio N, Inada H, Kang L, Yu Y, Ma D, Xu T, et al. C. elegans phototransduction requires a G protein-dependent cGMP pathway and a taste receptor homolog. Nat. Neurosci. 2010; 13:715–722. [PubMed: 20436480]

Mello C, Fire A. DNA transformation. Methods Cell Biol. 1995; 48:451–482. [PubMed: 8531738]

Mori I, Ohshima Y. Neural regulation of thermotaxis in Caenorhabditis elegans. Nature. 1995

Murai KK, Nguyen LN, Irie F, Yamaguchi Y, Pasquale EB. Control of hippocampal dendritic spine morphology through ephrin-A3/EphA4 signaling. Nat. Neurosci. 2003; 6:153–160. [PubMed: 12496762]

Murmu RP, Li W, Szepesi Z, Li J-Y. Altered Sensory Experience Exacerbates Stable Dendritic Spine and Synapse Loss in a Mouse Model of Huntington's Disease. J. Neurosci. 2015; 35:287–298. [PubMed: 25568121]

Penzes P, Cahill ME, Jones Ka, VanLeeuwen J-E, Woolfrey KM. Dendritic spine pathology in neuropsychiatric disorders. Nat. Neurosci. 2011; 14:285–293. [PubMed: 21346746]

Perkins, La; Hedgecock, EM.; Thomson, JN.; Culotti, JG. Mutant sensory cilia in the nematode Caenorhabditis elegans. Dev. Biol. 1986; 117:456–487. [PubMed: 2428682]

Perrault I, Rozet JM, Gerber S, Ghazi I, Ducroq D, Souied E, Leowski C, Bonnemaison M, Dufier JL, Munnich a, et al. Spectrum of retGC1 mutations in Leber's congenital amaurosis. Eur. J. Hum. Genet. 2000; 8:578–582. [PubMed: 10951519]

Potter LR. Regulation and therapeutic targeting of peptide-activated receptor guanylyl cyclases. Pharmacol. Ther. 2011; 130:71–82. [PubMed: 21185863]

Procko C, Lu Y, Shaham S. Glia delimit shape changes of sensory neuron receptive endings in C. elegans. Development. 2011; 138:1371–1381. [PubMed: 21350017]

Ramot D, MacInnis BL, Goodman MB. Bidirectional temperature-sensing by a single thermosensory neuron in C. elegans. Nat. Neurosci. 2008; 11:908–915. [PubMed: 18660808]

Russell JM. Sodium-Potassium-Chloride Cotransport. 2000; 80:211–276.

Satoh, a; Tokunaga, F.; Kawamura, S.; Ozaki, K. In situ inhibition of vesicle transport and protein processing in the dominant negative Rab1 mutant of Drosophila. J. Cell Sci. 1997; 110(Pt 2): 2943–2953. [PubMed: 9359879]

Satterlee JS, Sasakura H, Kuhara A, Berkeley M, Mori I, Sengupta P. Specification of thermosensory neuron fate in C. elegans requires ttx-1, a homolog of otd/Otx. Neuron. 2001; 31:943–956. [PubMed: 11580895]

Shaham S. Chemosensory organs as models of neuronal synapses. Nat. Rev. Neurosci. 2010; 11:212–217. [PubMed: 20029439]

Shyjan, aW; de Sauvage, FJ.; Gillett, Na; Goeddel, DV.; Lowe, DG. Molecular cloning of a retina-specific membrane guanylyl cyclase. Neuron. 1992; 9:727–737. [PubMed: 1356371]

Smith, Ba; Padrick, SB.; Doolittle, LK.; Daugherty-Clarke, K.; Corrêa, IR.; Xu, MQ.; Goode, BL.; Rosen, MK.; Gelles, J. Three-color single molecule imaging shows WASP detachment from Arp2/3 complex triggers actin filament branch formation. Elife. 2013a; 2013:1–25.

Smith HK, Luo L, O'Halloran D, Guo D, Huang X-Y, Samuel ADT, Hobert O. Defining specificity determinants of cGMP mediated gustatory sensory transduction in Caenorhabditis elegans. Genetics. 2013b; 194:885–901. [PubMed: 23695300]

Strauss O. The Retinal Pigment Epithelium in Visual Function. Physiol. Rev. 2005:845–881. [PubMed: 15987797]

Tan PL, Barr T, Inglis PN, Mitsuma N, Huang SM, Garcia-Gonzalez MA, Bradley BA, Coforio S, Albrecht PJ, Watnick T, et al. Loss of Bardet Biedl syndrome proteins causes defects in peripheral sensory innervation and function. Proc. Natl. Acad. Sci. U. S. A. 2007; 104:17524–17529. [PubMed: 17959775]

Tanis JE, Bellemer A, Moresco JJ, Forbush B, Koelle MR. The potassium chloride cotransporter KCC-2 coordinates development of inhibitory neurotransmission and synapse structure in Caenorhabditis elegans. J. Neurosci. 2009; 29:9943–9954. [PubMed: 19675228]

Thompson DK, Garbers D. Dominant negative mutation of the guanylyl cyclase-A receptor. J. Biol. Chem. 1995

Tong X, Ao Y, Faas GC, Nwaobi SE, Xu J, Haustein MD, Anderson Ma, Mody I, Olsen ML, Sofroniew MV, et al. Astrocyte Kir4.1 ion channel deficits contribute to neuronal dysfunction in Huntington's disease model mice. Nat. Neurosci. 2014; 17:694–703. [PubMed: 24686787]

Tora AS, Rovira X, Dione I, Bertrand H-O, Brabet I, De Koninck Y, Doyon N, Pin J-P, Acher F, Goudet C. Allosteric modulation of metabotropic glutamate receptors by chloride ions. FASEB J. 2015; 29:4174–4188. [PubMed: 26116702]

Wang D, O'Halloran D, Goodman MB. GCY-8, PDE-2, and NCS-1 are critical elements of the cGMP-dependent thermotransduction cascade in the AFD neurons responsible for C. elegans thermotaxis. J. Gen. Physiol. 2013; 142:437–449. [PubMed: 24081984]

Ward S, Thomson N, White JG, Brenner S. Electron microscopical reconstruction of the anterior sensory anatomy of the nematode Caenorhabditis elegans.?2UU. J. Comp. Neurol. 1975; 160:313–337. [PubMed: 1112927]

Wasserman SM, Beverly M, Bell HW, Sengupta P. Regulation of response properties and operating range of the AFD thermosensory neurons by cGMP signaling. Curr. Biol. 2011; 21:353–362. [PubMed: 21315599]

Wedel BJ, Foster DC, Miller DE, Garbers DL. A mutation of the atrial natriuretic peptide (guanylyl cyclase-A) receptor results in a constitutively hyperactive enzyme. Proc. Natl. Acad. Sci. U. S. A. 1997; 94:459–462. [PubMed: 9012805]

Yu S, Avery L, Baude E, Garbers DL. Guanylyl cyclase expression in specific sensory neurons: a new family of chemosensory receptors. Proc. Natl. Acad. Sci. U. S. A. 1997; 94:3384–3387. [PubMed: 9096403]
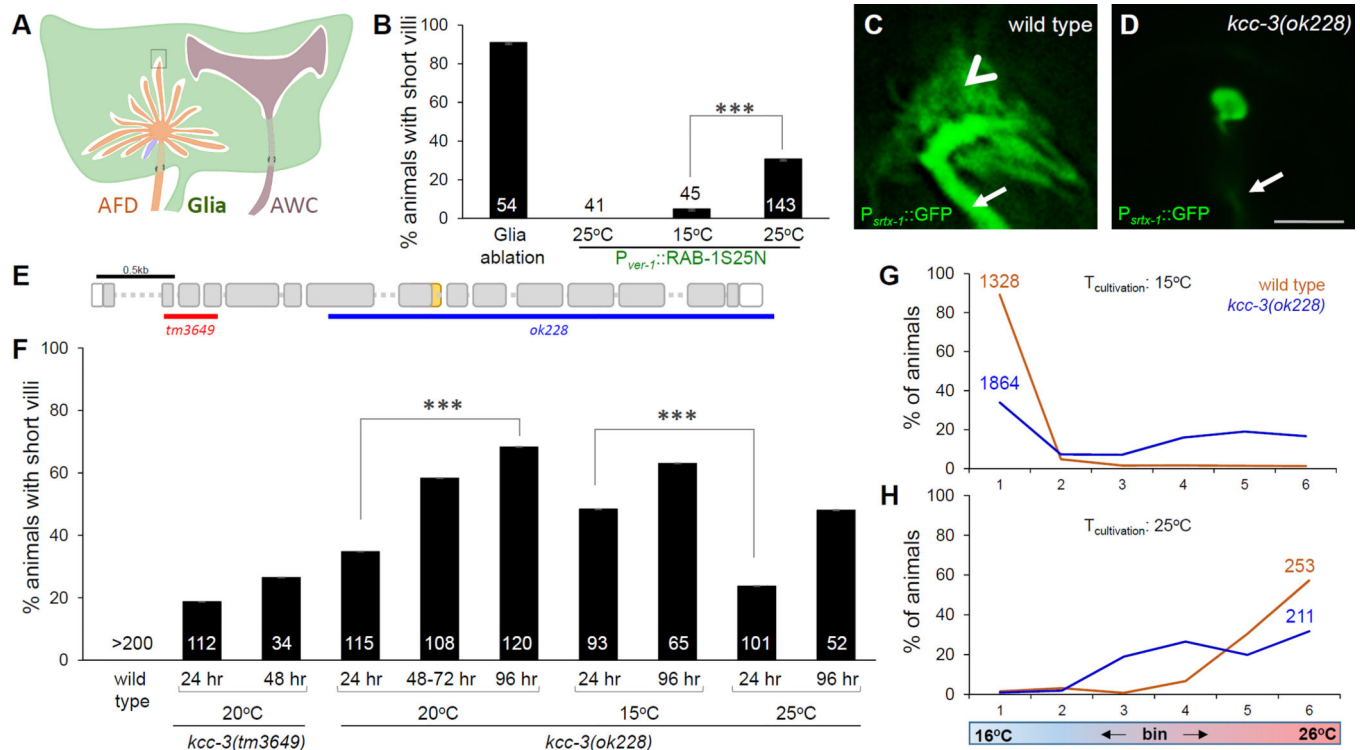
Figure 1. Glial KCC-3 controls AFD neuron receptive-ending shape

(A) AMsh glia ensheathes multiple neurons. AFD (orange) also has a cilium (blue). Boxed region magnified in Figure 7. (B) Histogram depicting AFD defects in indicated genotypes. Numbers, animals scored. Error bars, SEM. ***p<0.0002. For transgenics, three independent lines were scored. Green text, glia expression; red text, AFD expression. Second bar, non-transgenic siblings (C,D) Fluorescence images of wild-type (C) and *kcc-3*(*ok228*) (D) AFD microvilli. Scale bar, 1μm. Arrow, dendritic shaft. Arrowhead, microvilli. (E) *kcc-3* gene structure, deletions used are indicated by red and blue bars. Sequences not included in WormBase annotation, orange. (F) Histogram details as in Figure 1B. Time, hours post mid L4 stage. (G, H) Thermotaxis behavior assays for indicated genotype raised at 15°C (G) and 25°C (H). Animals in (G), 24 hours post mid-L4 stage. Animals in (H), 96 hours post mid-L4 stage. N, Number of animals. See also Figure S1 and S2.
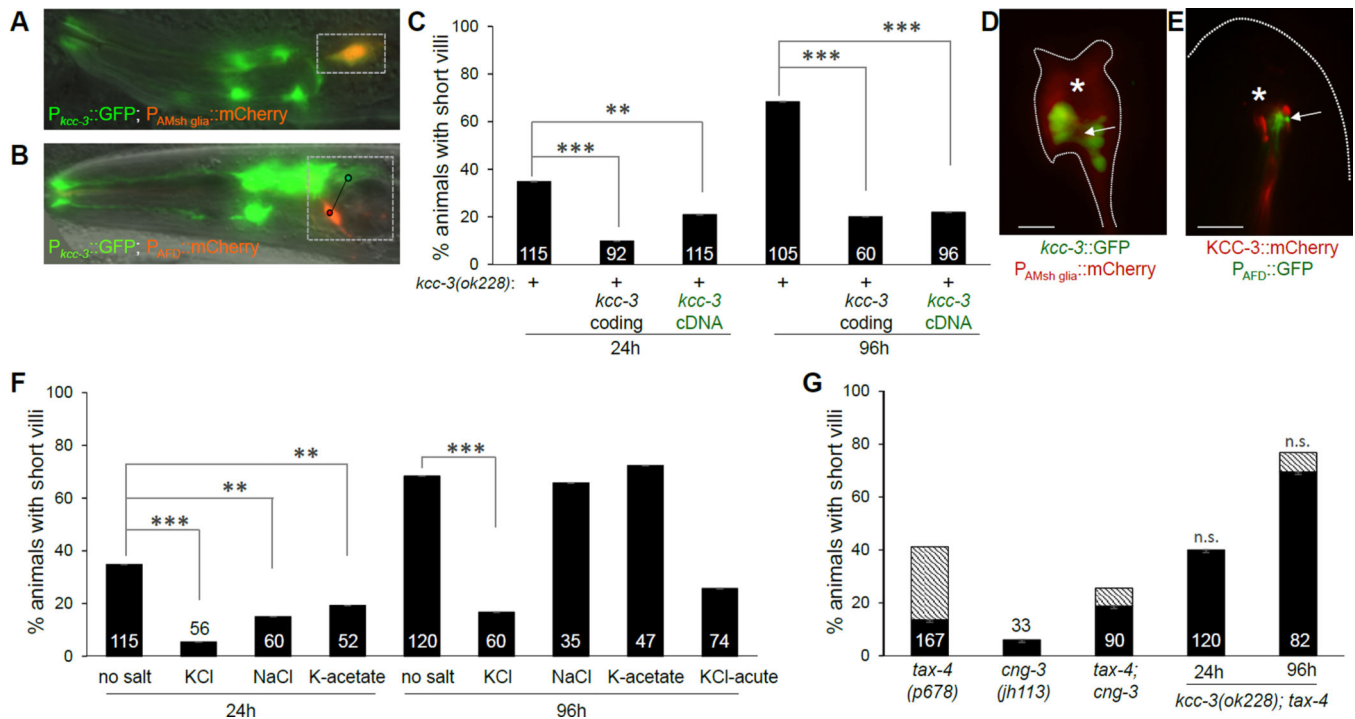
Figure 2. KCC-3 localizes to glial membranes surrounding AFD and regulates KCl homeostasis
(A,B) Fluorescence images depicting expression of indicated transcriptional reporters. Box, cells of interest. Circles + line in (B) indicate distinct cells. (C) Histogram details as in 1B and 1F. +, presence of *kcc-3(ok228)* allele. **p=0.009. (D, E) Arrow, AFD receptive-ending region. Asterisk, location of AWC cilium. (F, G) Histogram details as in 1B and 1F. **p<0.02. n.s., not significant compared to age-matched *kcc-3(ok228)*. Hatched bars, animals with disorganized AFD microvilli.
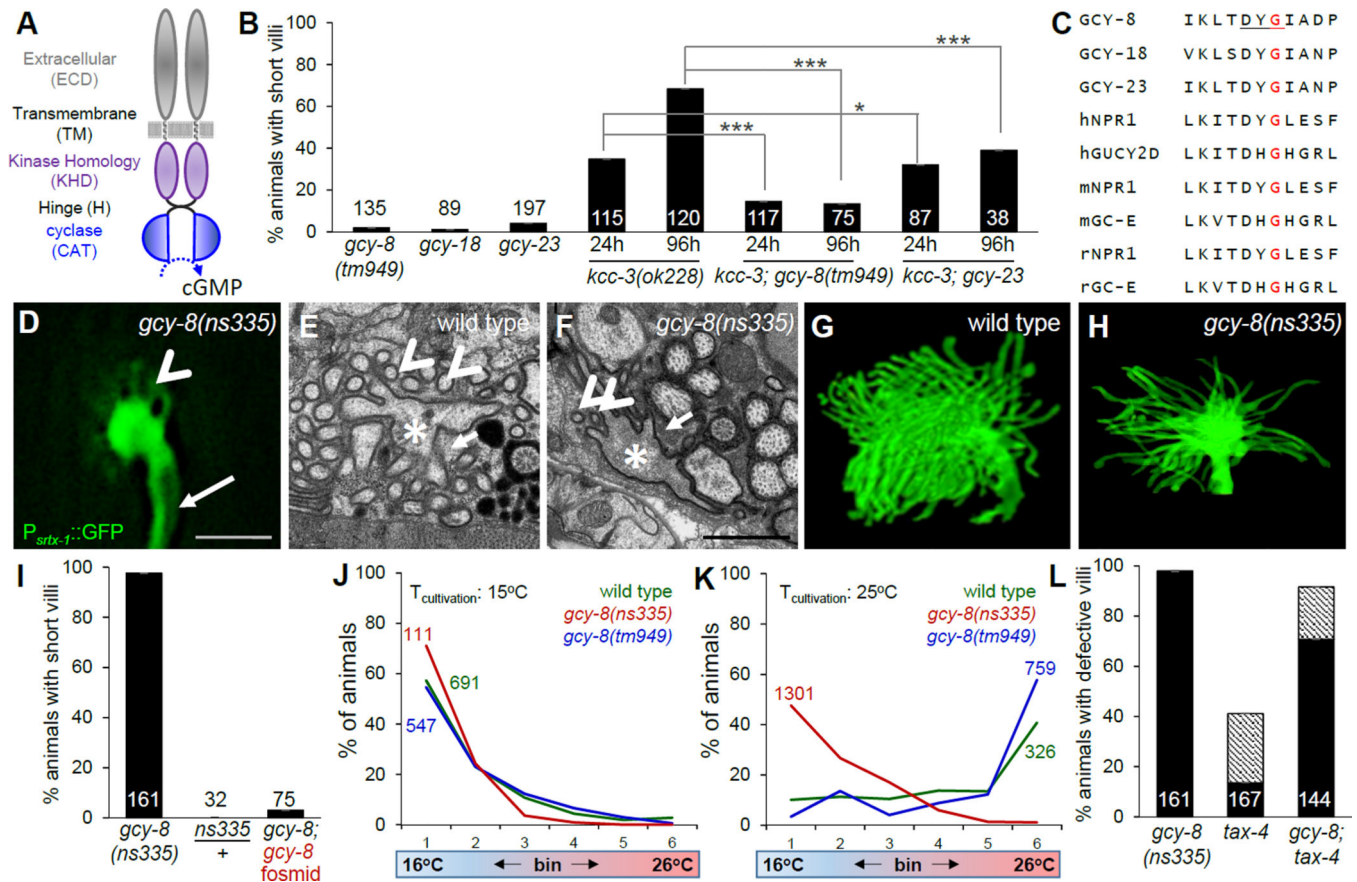
**Figure 3. The neuronal rGC GCY-8 functions downstream of glial KCC-3**

(A) GCY-8 domain structure. (B) Histogram details as in 1B and 1F. *p=0.34. (C) Partial alignment of GCY-8. Red, conserved glycine mutated in *gcy-8(ns335)*. (D,F,H) Fluorescence, TEM, and FIB-SEM reconstruction, respectively, of *gcy-8(ns335)* AFD receptive-ending. (E, G) TEM and FIB-SEM reconstruction, respectively, of wild-type AFD receptive-ending. (D) Arrow, dendritic shaft. Arrowhead, short microvilli. (E,F) Arrowheads, microvilli. Asterisk, dendritic shaft. Arrow, glial cytosol. Scale bar, 1μm. (I) Histogram details as in 1B. (J, K) Thermotaxis assays as in 1G. Animals raised at 15°C (J) or 25°C (K). (L) Histogram as in 1B. Hatched, animals with disorganized microvilli. See also Figure S3, S4 and Movies 1–4.
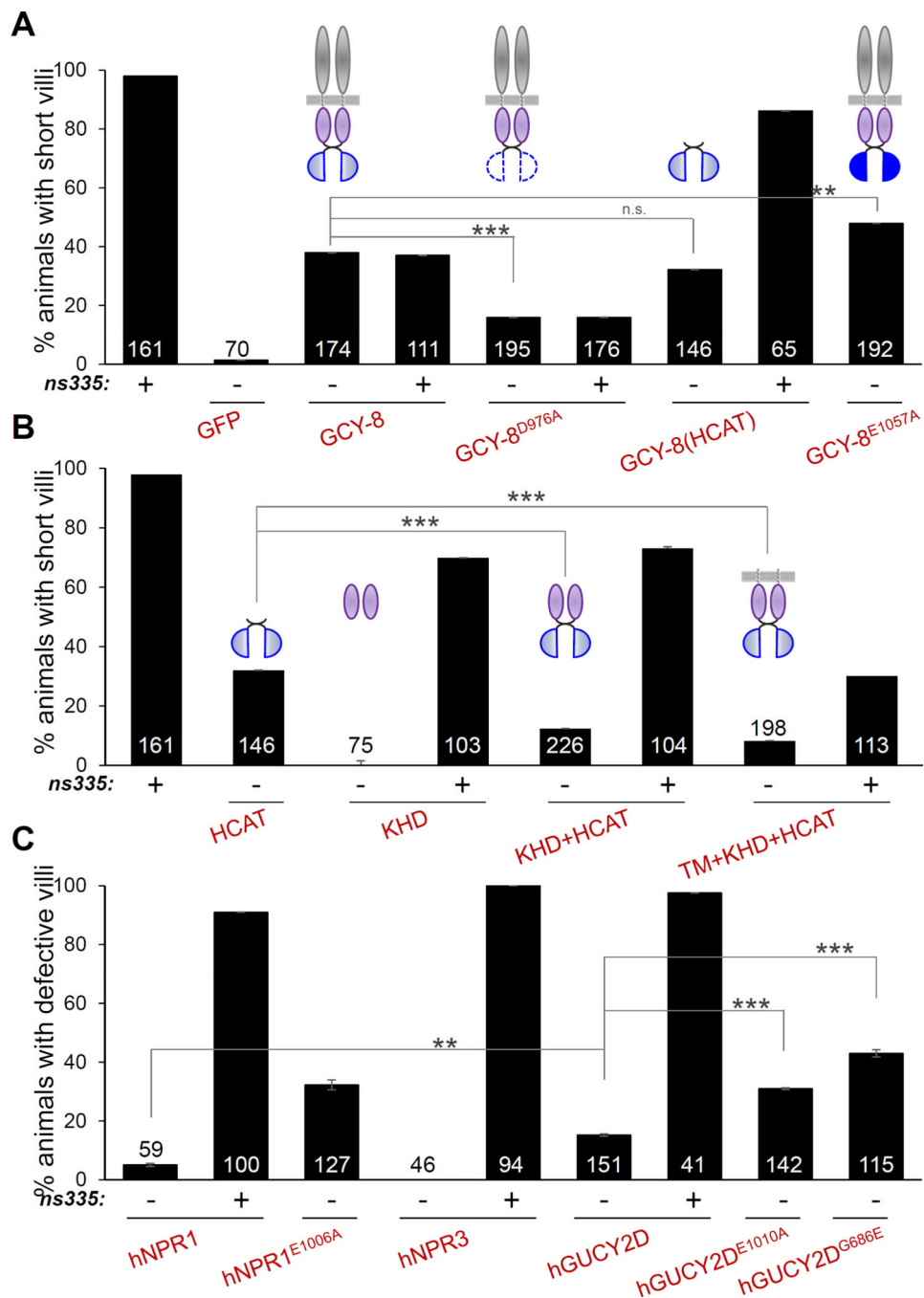
Figure 4. Excess GCY-8 and cGMP cause loss of AFD receptive-ending
Histogram details are as in Figure 1B. +, –, presence or absence, respectively, of
gcy-8(ns335). Diagrams depict overexpressed GCY-8 protein. White-blue, weak-strong
predicted cyclase activity (A). **p<0.02. n.s., not significant.
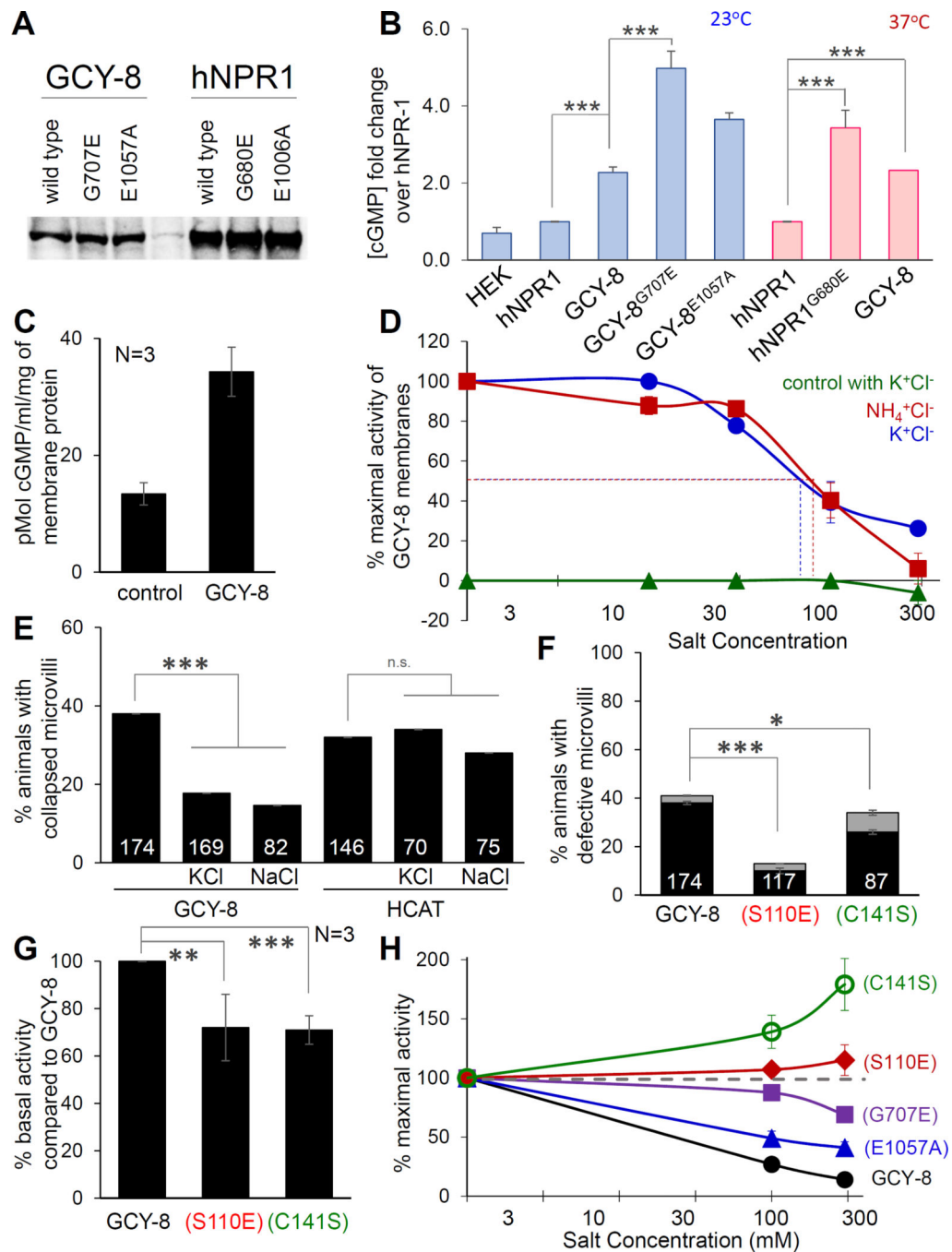
Figure 5. Chloride inhibits GCY-8 cyclase basal activity

(A) Western blot showing expression of indicated rGC proteins in HEK239T cells. (B) Histogram showing steady-state cGMP levels in HEK239T cells expressing the indicated constructs. Error bars, SEM of 3–4 experiments. ***p<0.0008. (C) cGMP measurements in membrane fractions of control HEK293T cells or GCY-8-expressing HEK293T cells. (D) Inhibition of GCY-8 membrane fraction guanylyl cyclase activity by chloride. Dotted lines, half-maximal effect. X-axis is plotted on a $\log_{10}$ scale. (E, F) Histogram details as in Figure 1B. (F) Mutations engineered in full-length GCY-8 noted in color, see also Figure
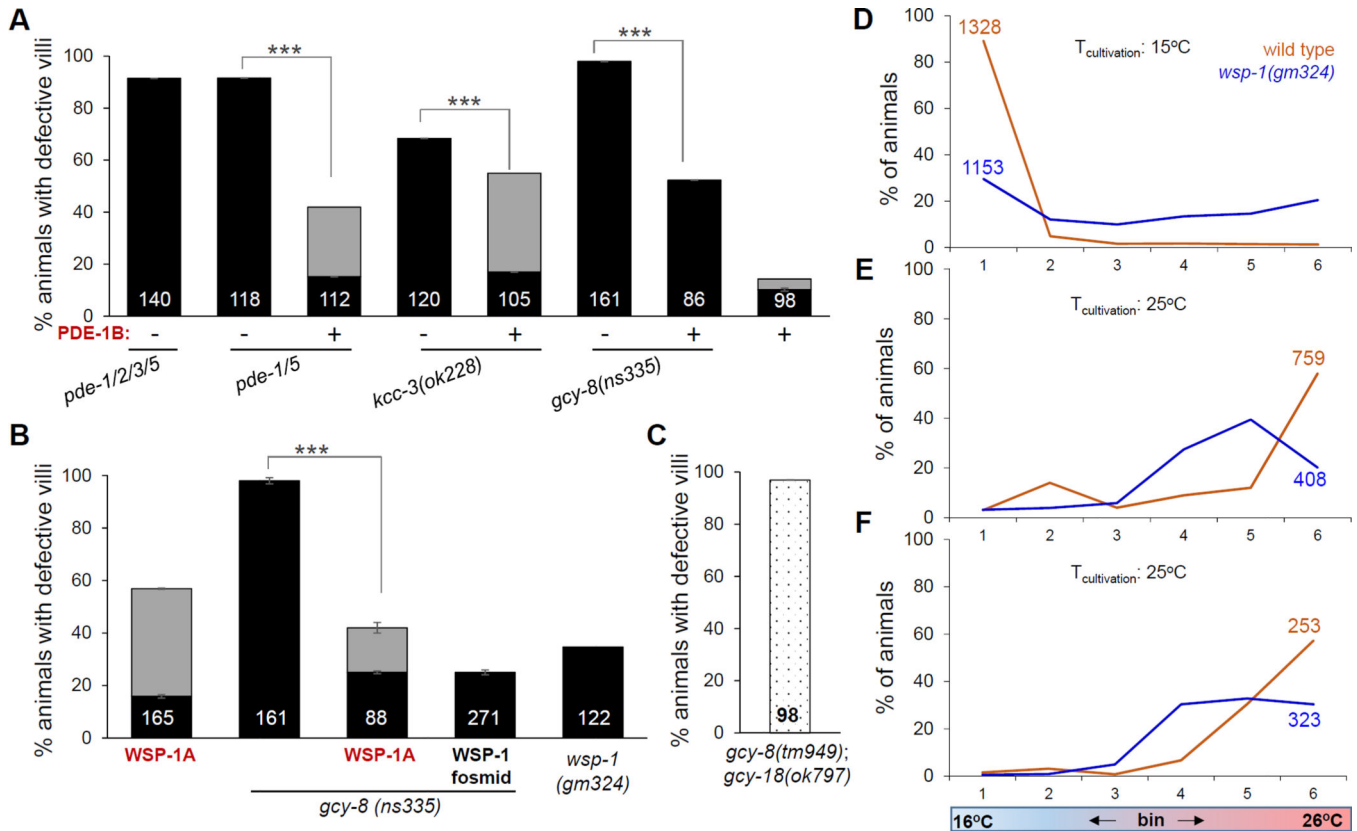
S5C.*=p<0.03 (G) Histogram details as in Figure 5C. Mutations noted as in Figure 5F.
***p=0.004; **p=0.01 (H) Details as in Figure 5D and 5F. Activity of each protein
normalized to basal activity in 0mM NH4$^+$Cl$^-$ (dashed grey line). See also Figure S5.

Figure 6. The actin regulator WSP-1 regulates AFD shape downstream of GCY-8

(A–C) Histogram details as in Figure 1B. (A)+/−, presence or absence, respectively of PDE-1B over-expression (B) Gray, animals with extended microvilli. (C) Dotted, animals with slightly shorter, but not absent, microvilli. (D–F) Thermotaxis assays as in Figure 1G. 24 hours post mid-L4 stage animals raised at 15°C (D) or 25°C (E), and 96 hours post mid-L4 stage animals raised at 25°C (F). See also Figure S6 and S7.
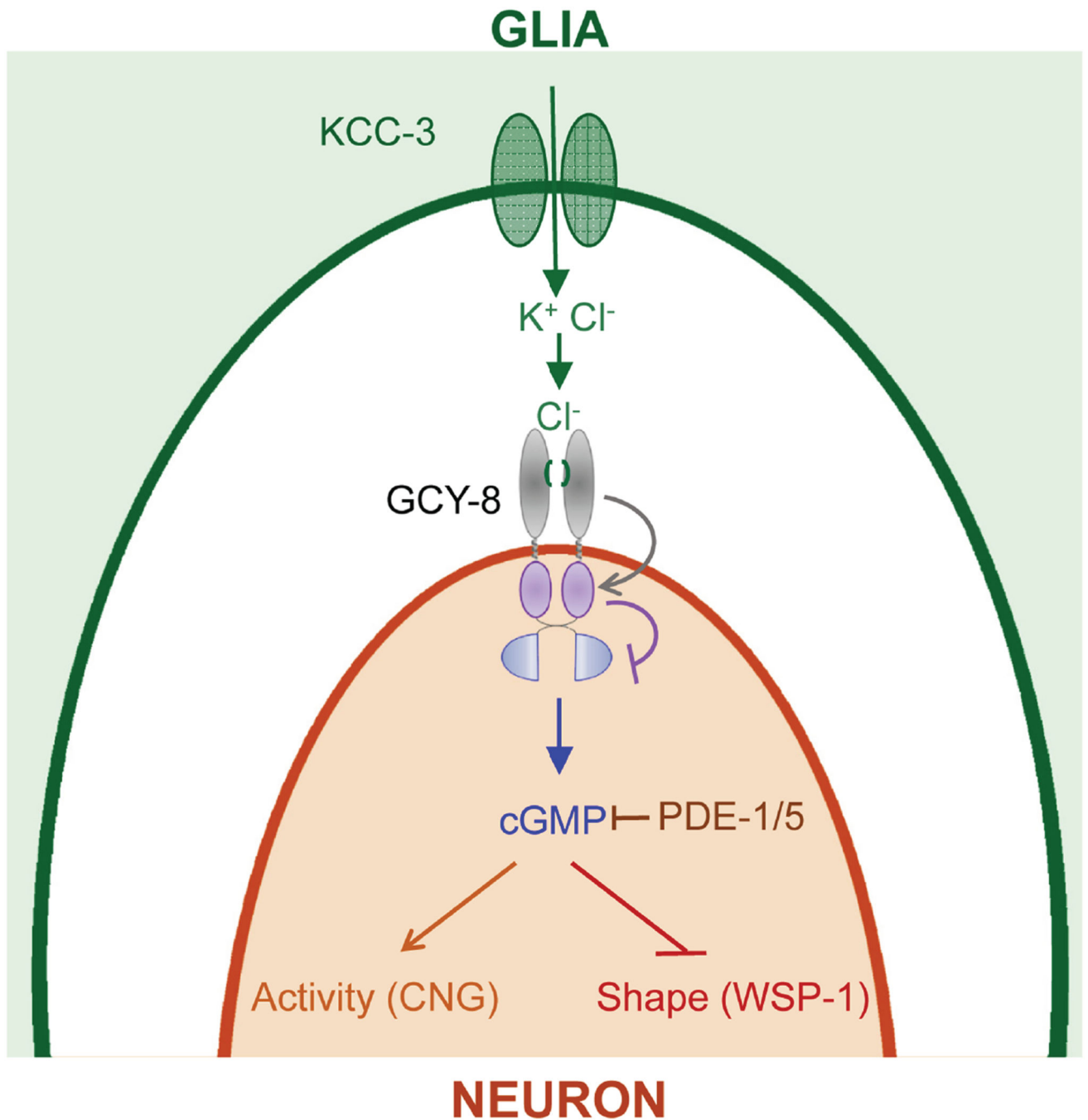
Figure 7. Model for AFD neuron receptive-ending shape control by AMsh glia
Magnified view of boxed region in Figure 1A. Glial KCC-3 regulates chloride in the extracellular milieu around AFD receptive-ending. Chloride inhibits GCY-8 by binding the $S(x)_nGPxC$ motif in its ECD. GCY-8, PDE-1 and PDE-5 control cGMP levels, which antagonizes the actin cytoskeleton through WSP-1.